molecule) also destabilized it, suggesting that the repeats are a module for protein destabilization. These results indicate that the intracellular distribution of Cfr is regulated by two distinct mechanisms. First, the transmembrane region and cytoplasmic tail retain Cfr in the Golgi apparatus, and secondly the extracellular juxtamembrane Cfr repeats destabilize Cfr passed through the Golgi apparatus, allowing Cfr to exhibit its unique multiple functions.

MATERIALS AND METHODS

cDNAs

In all of the mutants of Cfr used in the present study, the signal sequence of mouse Cfr (amino acids 1–27) was replaced by the signal sequence of mouse CD2 and a FLAG tag. FLAG–CfrΔ1169, corresponding to the reported rat Δ1165 mutant [10], was generated by deleting the C-terminal six amino acid residues (RELKDR). In all of the GPI-anchored mutants, the extracellular domain of Cfr (amino acids 1–1141) was fused to the signal sequence for the GPI-anchor of human CD58 [also known as LFA (leucocyte function-associated antigen) 3, amino acids 204–237] [13]. In FLAG–Cfr–KARA–GPI, KR (amino acids 1096–1097) and KKR (amino acids 1105–1107) were replaced with AA and AAA respectively. In FLAG–CfrΔ13–16–GPI and FLAG–CfrΔ13–16, Cfr repeats 13–16 (amino acids 870–1141) were deleted. Similarly, in FLAG–CfrΔ15–16–GPI and FLAG–CfrΔ16–GPI, repeats 15 and 16 (amino acids 995–1141) and repeat 16 (amino acids 1057–1141) were deleted. In EpCAM–CfrRepeat, Cfr repeats 13–16 were inserted between the C-terminus of the extracellular domain and the N-terminus of the transmembrane region of mouse EpCAM (between amino acids 266 and 267).

Antibodies

The antibodies used were as follows: anti-FLAG M2 antibody (F3165) from Sigma, anti-actin antibody (sc-1616) from Santa Cruz Biotechnology, anti-TGOLN2 (*trans*-Golgi network protein 2, also known as Tgn38 and Tgn46) antibody (ab16059) and anti-EpCAM antibody (for Western blot analysis) (ab32392) from Abcam, and anti-EpCAM antibody (for immunofluorescent staining) (552370) from BD Pharmingen. The rabbit serum against Cfr and a rat monoclonal antibody against EpCAM (for flow cytometry) have been described previously [3,14].

Inhibition of lysosomes and proteasomes

Ba/F3 cells were incubated in medium containing 10 mM NH_4Cl (Wako) as a lysosomal enzyme inhibitor, or 10 mM MG-132 (Sigma) as a proteasome inhibitor at 37 °C for 12 h. In parallel with these treatments, Ba/F3 cells were also incubated in medium with PBS and DMSO as a control. The cells were then either harvested for Western blot analysis or analysed by flow cytometry for cell-surface expression of the FLAG-tagged Cfr proteins.

Retroviral infection and proliferation of Ba/F3 cells

Ba/F3 cells and NIH 3T3 cells were infected with retroviruses containing cDNA for a Cfr mutant with an IRES (internal ribosomal entry site)–EGFP (enhanced green fluorescent protein) sequence. The methods used for the proliferation assay have been described previously [3]. Briefly, we sorted EGFP-positive Ba/F3 cells by FACSVantage (BD), and performed the assay in 96-well plates with WST-1 (water-soluble tetrazolium salt 1; Roche Applied Science). GST (glutathione transferase) and GST–Fgf18 used in the present study were described previously [3].

Protein stability assay

Ba/F3 cells were incubated with 50 μg/ml cycloheximide for different periods of time and then harvested for Western blot analysis.

Immunofluorescent staining

Ba/F3 cells were fixed with 4 % paraformaldehyde in PBS at room temperature (25 °C) for 10 min. The cells were incubated with primary antibodies in 5 % skimmed milk in PBS at 4 °C overnight. They were then incubated with secondary antibodies in 5 % skimmed milk in PBS at room temperature for 2 h, and embedded in GEL/MOUNT (Biomeda) containing Hoechst 33342. Signals were observed under a confocal microscope.

Biotin-labelling assay

Ba/F3 cells were washed three times with ice-cold PBS with 0.7 mM $CaCl_2$ and 0.5 mM $MgCl_2$. Biotinylation of cell-surface proteins was performed with 500 μl of 300 μg/ml EZ-Link-Sulfo-NHS-SS-biotin (Pierce) in PBS for 30 min at 4 °C. Unbound biotin was removed by three washes with ice-cold PBS. Biotinylated cells were incubated with 500 μl of lysis buffer [50 mM Tris/HCl (pH 7.5), 150 mM NaCl, 1 % Nonidet P40, 1 mM EDTA, 1 μg/ml leupeptin (Roche Applied Science), 1 mM PMSF (Wako) and 500 μg/ml Pefabloc (Roche Applied Science)] for 1 h at 4 °C. Immuno-Pure immobilized streptavidin (Pierce) was then added to biotinylated cell lysate and incubated for 2 h at 4 °C to pull down the biotin-labelled proteins. After washing three times with the lysis buffer, the resins were boiled and the pulled down proteins were subjected to Western blot analysis.

Western and Northern blot analyses

The methods used for the Western and Northern blot analyses have been described previously [15].

RESULTS

Intracellular distribution of Cfr in Ba/F3 cells

We reported previously that forced expression of Cfr enhanced Fgf18 signalling via Fgfr3c in Ba/F3 cells [3]. Cfr, however, has been known as a protein of the Golgi apparatus, so we investigated the intracellular distribution of Cfr by expressing the protein with a FLAG tag at its N-terminus (FLAG–Cfr) in Ba/F3 cells (Figure 1A). Flow cytometric analysis with an anti-FLAG antibody showed that FLAG–Cfr was significantly expressed on the cell surface (Figure 1B). By contrast, immunofluorescent microscopic observation with the anti-FLAG antibody revealed that FLAG–Cfr occurred predominantly in the Golgi apparatus, whereas its expression on the cell surface was barely detectable (Figure 1C).

Cfr lacking the cytoplasmic tail enhances Fgf18 signalling on the cell surface

Because FLAG–Cfr was located both on the cell surface and in the Golgi apparatus, it was not clear where Cfr functions in Fgf18 signalling. Therefore we attempted to restrict Cfr to the

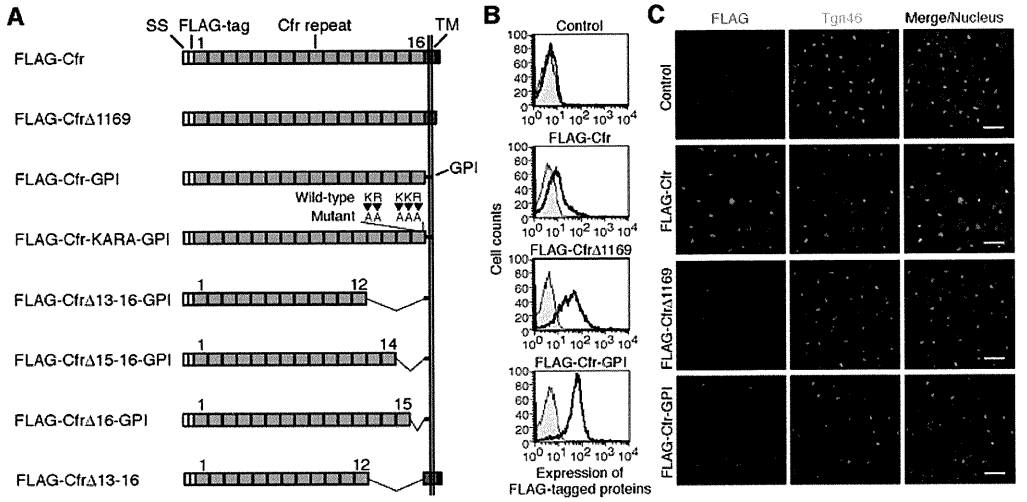

Figure 1 Intracellular distribution of the C-terminally modified Cfr mutants in Ba/F3 cells

(**A**) Schematic representation of the Cfr mutants. All of the mutant proteins have a FLAG tag at their N-terminus. The GPI-anchored mutants have a GPI signal sequence by which they are recruited to the cell surface via GPI. Deleted regions and point-mutated sites are also indicated. SS, signal sequence; TM, transmembrane domain. (**B**) Expression of FLAG–Cfr, FLAG–CfrΔ1169 and FLAG–Cfr–GPI on the Ba/F3 cell surface monitored by flow cytometry. Ba/F3 cells with only EGFP were used as a control. Note that FLAG–Cfr was significantly expressed on the cell surface compared with the control cells, and the C-terminal modification enhanced the surface expression. The filled plot is the isotype control and open plot is the anti-FLAG. (**C**) Immunofluorescent staining of FLAG (red) in Ba/F3 cells. The Golgi apparatus was also visualized by staining of TGOLN2 (Tgn46, green). In the merged photographs, signals of FLAG, TGOLN2 and nuclei (blue) are merged. Scale bar, 20 μm.

cell surface. For this purpose, we generated two Cfr mutants by modifying the C-terminal domain, as it was reported that the C-terminal cytoplasmic region is required for the expression of Cfr in the Golgi apparatus [10]. One mutant was a FLAG-tagged Cfr without the C-terminal cytoplasmic tail (FLAG–CfrΔ1169), which corresponds to the rat Cfr mutant reported to be expressed on the cell surface [10] (Figure 1A). The other comprised the FLAG-tagged extracellular domain of Cfr fused to the well-characterized GPI signal peptide of human CD58 [13] (FLAG–Cfr–GPI) (Figure 1A). We expressed these two mutants in Ba/F3 cells, and monitored their intracellular distribution. As expected, the surface expression of these mutants was stronger than that of FLAG–Cfr, and they were barely detected in the Golgi apparatus (Figures 1B and 1C).

We then established Ba/F3 cells expressing Fgfr3c with either FLAG–Cfr or FLAG–Cfr–GPI to determine their response to Fgf18. Consistent with our previous report, FLAG–Cfr enhanced Fgf18 signalling via Fgfr3c in Ba/F3 cells (Figure 2). Furthermore, Ba/F3 cells with FLAG–Cfr–GPI, like those with FLAG–Cfr, more strongly responded to Fgf18 than control cells (Figure 2). These results suggest that the positive effect of Cfr on Fgf signalling is determined by its level of expression on the cell surface, not in the Golgi apparatus. Furthermore, the cytoplasmic tail is unnecessary for the function of Cfr in Fgf signalling.

Instability of the C-terminally modified Cfr mutants

As Cfr expressed on the cell surface enhances Fgf18 signalling, the regulation of its transport from the Golgi apparatus to the cell surface is important for its functions. Therefore we investigated further the regulatory mechanisms governing the intracellular distribution of Cfr.

We noticed that the cell-surface expression of the C-terminally modified mutants FLAG–CfrΔ1169 and FLAG–Cfr–GPI was rather weak and that it was under the detection limit of the biotin-labelling assay (Figure 1B and results not shown). Therefore we checked mRNA and protein levels and found that the amount of

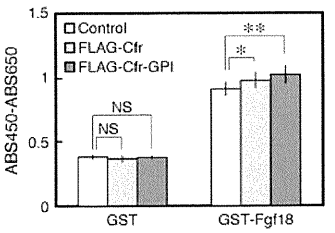

Figure 2 Effects of FLAG–Cfr–GPI on Fgf18 signalling

Ba/F3 cells expressing both Fgfr3c and FLAG–Cfr–GPI, as well as those with Fgfr3c and FLAG–Cfr were stimulated with 500 ng/ml GST (glutathione transferase)–Fgf18. The same amount of GST was added as a control. The extent of proliferation was monitored by WST-1 assay, and absorbance at 450 nm minus basal absorbance at 650 nm ± S.D. is shown. We prepared eight wells for each condition. FLAG–Cfr–GPI enhanced Fgf18 signalling like FLAG–Cfr. *P* value was calculated with Student's *t* test: * $P < 0.05$; ** $P < 0.01$; NS, $P > 0.2$.

protein was greatly reduced for FLAG–CfrΔ1169 and FLAG–Cfr–GPI compared with FLAG–Cfr, whereas the amount of mRNA was comparable with that for FLAG–Cfr (Figure 3A). The results indicate that these mutant proteins are unstable, raising the possibility that lysosomal or proteasomal degradation may occur. To address this possibility, a lysosomal enzyme inhibitor NH_4Cl or a proteasome inhibitor MG-132 were added to the cells. However, neither inhibitor rescued the total amount of FLAG–Cfr–GPI protein (Figure 3B). Moreover, these inhibitors failed to recover the cell-surface expression of FLAG–Cfr–GPI (Figure 3C). The results suggest that these Cfr mutants were destabilized by another mechanism.

Shedding of Cfr is not involved in the instability of the Cfr mutants

Because previous reports have shown that the extracellular domain of Cfr is cleaved in the juxtamembrane region to be secreted into the culture supernatant [8,12], we considered the possibility that the instability of Cfr is caused by shedding rather than degradation through the lysosome or proteasome. Therefore

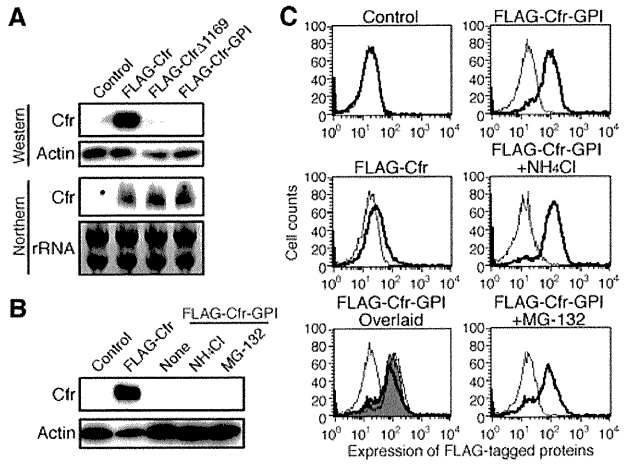

Figure 3 Protein and mRNA expression of the C-terminally modified mutants in Ba/F3 cells

(**A**) Western and Northern blot analyses of protein and mRNA expression of the C-terminal mutants in Ba/F3 cells. The total amount of protein and RNA loaded was monitored by blotting with an anti-actin antibody and visualization of rRNA with ethidium bromide respectively. The protein expression of the mutants is dramatically reduced compared with that of FLAG–Cfr, whereas the mRNA levels are comparable. Note that the endogenous full-length Cfr was also detected in all samples with anti-Cfr serum. (**B**) Effect of inhibitors for lysosomal enzymes or proteasomes on protein expression of FLAG–Cfr–GPI in Ba/F3 cells. Ba/F3 cells expressing FLAG–Cfr–GPI were incubated with a lysosomal enzyme inhibitor (NH_4Cl), a proteasome inhibitor (MG-132) or solvent (None) for 12 h. (**C**) Effect of NH_4Cl and MG-132 on the cell-surface expression of FLAG–Cfr–GPI. The cell-surface expression of FLAG–Cfr–GPI in Ba/F3 cells treated with NH_4Cl and MG-132 was analysed by flow cytometry. For each sample: filled, isotype controls; open, anti-FLAG. For the lower left-hand panel: filled, isotype control of None (light grey), anti-FLAG of None (dark grey) and overlaid, NH_4Cl (thin line), and MG-132 (bold line). Neither inhibitor recovered the protein expression of FLAG–Cfr–GPI.

we investigated the amount of the shed extracellular domain of Cfr in the culture supernatants of Ba/F3 cells expressing FLAG–Cfr or FLAG–Cfr–GPI. We immunoprecipitated the extracellular domain from the culture supernatants by the anti-FLAG antibody. As shown in Figure 4(A), the amounts of proteins precipitated were comparable between FLAG–Cfr and FLAG–Cfr–GPI, whereas the amount of FLAG–Cfr–GPI in the cell lysate was extremely low compared with that of FLAG–Cfr, indicating that the shedding of the extracellular domain was not a main cause of the instability. As there are two potential basic proteolytic cleavage sites in the juxtamembrane region of Cfr [8], we investigated further the involvement of shedding in the protein instability by introducing point mutations into FLAG–Cfr–GPI to replace the basic sites KR and KKR with an alanine residue (FLAG–Cfr–KARA–GPI) (Figure 1A). We expressed the mutant in Ba/F3 cells and monitored its expression. Flow cytometric analysis showed that there was no difference in cell-surface expression between FLAG–Cfr–GPI and FLAG–Cfr–KARA–GPI (Figure 4B). Although Northern blot analysis showed that the mRNA levels of FLAG–Cfr–KARA–GPI and FLAG–Cfr–GPI were comparable, and greater than that of FLAG–Cfr, the protein levels were not increased by the mutation (Figure 4C). These results clearly indicate that proteolytic cleavage in the juxtamembrane region is not involved in the instability of the Cfr mutants with the C-terminal modification.

Cfr repeats in the juxtamembrane region destabilize Cfr

Because the basic amino acid sites in the juxtamembrane region do not appear to destabilize Cfr, we examined a possibility that the stability of Cfr is regulated by the Cfr repeats. For this purpose we generated deletion mutants. As shown in Figure 1(A), the extracellular domain of Cfr is composed of 16 repeats of a unique motif, the Cfr repeat. First, we deleted repeats 13–16 from FLAG–Cfr–GPI (FLAG–CfrΔ13–16–GPI) (Figure 1A), and expressed the mutant in Ba/F3 cells. Surprisingly, FLAG–CfrΔ13–16–GPI was expressed more strongly on the cell surface than FLAG–Cfr–GPI, and FLAG–CfrΔ13–16–GPI was clearly detected by Western blotting unlike FLAG–Cfr–GPI (Figures 4A, 5A and 5B). Therefore the deleted juxtamembrane domain is critical for the stability of Cfr. To narrow down the region, we generated two additional mutants FLAG–CfrΔ15–16–GPI and FLAG–CfrΔ16–GPI in which the last two repeats and last repeat were deleted from FLAG–Cfr–GPI respectively (Figure 1A), and expressed them in Ba/F3 cells. Unexpectedly, FLAG–CfrΔ15–16–GPI and FLAG–CfrΔ16–GPI were expressed on the cell surface at levels in between those of FLAG–Cfr–GPI and FLAG–CfrΔ13–16–GPI (Figure 5A). Overlaying the flow cytometric profiles clearly showed that the GPI-anchored mutants with fewer Cfr repeats exhibited stronger expression on the cell surface (Figure 5A). We also detected FLAG–CfrΔ15–16–GPI and FLAG–CfrΔ16–GPI by Western blotting, indicating that these mutants were more stable than FLAG–Cfr–GPI (Figure 5B). Furthermore, immunofluorescent staining revealed increased cell-surface expression of FLAG–CfrΔ13–16–GPI compared with FLAG–Cfr–GPI (Figure 5C). On the basis of these results, we concluded that without the C-terminal domain, more Cfr is recruited to the cell surface from the Golgi apparatus, but the juxtamembrane Cfr repeats destabilize the Cfr protein, reducing its cell-surface expression.

Cfr protein is unstable outside the Golgi apparatus

To investigate the instability of Cfr protein more directly, we determined the half-lives of the Cfr mutants. For this purpose, we added cycloheximide to Ba/F3 cells expressing the Cfr mutants and monitored their amounts by Western blot analysis. The full-length Cfr was stable and the protein level was not changed significantly, even after 5 h in this assay (Figure 6A). By contrast, the protein level of FLAG–Cfr–GPI was too low to determine the half-life in this assay (Figures 3A and 3B, and results not shown). Therefore we determined the half-lives of the Cfr mutants with intermediate stability, FLAG–CfrΔ13–16–GPI and FLAG–CfrΔ15–16–GPI. In contrast with the full-length Cfr, these mutants were unstable and their amounts declined by the addition of cycloheximide (Figure 6A). On the basis of three independent experiments, the half-lives of FLAG–CfrΔ13–16–GPI and FLAG–CfrΔ15–16–GPI were estimated to be 102.6 and 92.7 min respectively (Figure 6B). These results clearly show that Cfr is stable in the Golgi apparatus, whereas it is highly unstable outside the Golgi apparatus.

Retention of Cfr in the Golgi apparatus through its C-terminus prior to destabilization by the Cfr repeats

We then deleted the Cfr repeats 13–16 from FLAG–Cfr (FLAG–CfrΔ13–16) (Figure 1A), and expressed the mutant in Ba/F3 cells. The level of FLAG–CfrΔ13–16 on the cell surface was comparable with that of FLAG–Cfr in the flow cytometric analysis (Figure 7A). Western blot analysis revealed that the amount of protein was also comparable with that of FLAG–Cfr, and robustly increased compared with that of FLAG–CfrΔ13–16–GPI (Figure 7B). Moreover, we observed that FLAG–CfrΔ13–16 was mostly present in the Golgi apparatus like FLAG–Cfr,

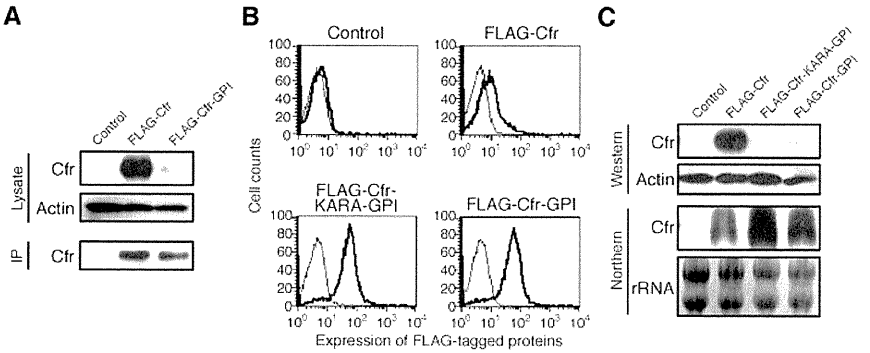

Figure 4 Expression of the Cfr with mutations in the juxtamembrane basic sites

(**A**) Secretion of the extracellular domain of Cfr into the culture supernatants of Ba/F3 cells. The extracellular domain was immunoprecipitated from the culture supernatants of Ba/F3 cells expressing FLAG–Cfr or FLAG–Cfr–GPI, and then subjected to Western blot analysis (IP). Expression of Cfr in Ba/F3 cells and the total amount of the cell lysate loaded was monitored by blotting with anti-Cfr serum and anti-actin antibody respectively (Lysate). The amount of the extracellular domain secreted was comparable between FLAG–Cfr and FLAG–Cfr–GPI. (**B**) Cell-surface expression of FLAG–Cfr–KARA–GPI. Filled, isotype control; open, anti-FLAG. No difference in the expression level was observed between FLAG–Cfr–KARA–GPI and FLAG–Cfr–GPI. (**C**) The total amount of FLAG–Cfr–KARA–GPI protein and mRNA in Ba/F3 cells. Mutations in the two basic sites did not alter the amount of total protein expression from FLAG–Cfr–GPI.

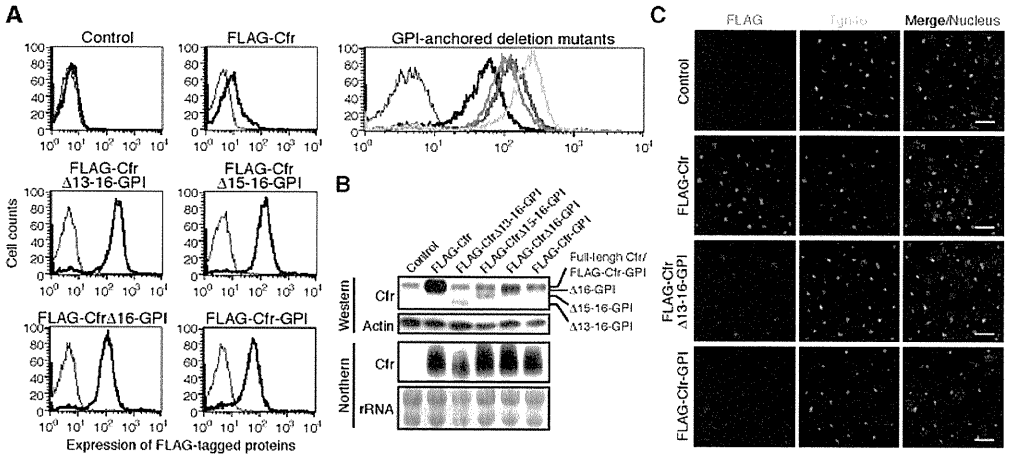

Figure 5 Expression of the mutants deleted of the Cfr repeats in Ba/F3 cells

(**A**) Flow cytometric analysis of the GPI-anchored deletion mutants. Cell-surface expression of the mutants was monitored using the FLAG tag. For each sample: filled, isotype control; open, anti-FLAG. For the panel showing GPI-anchored deletion mutants: filled, isotype control of FLAG–Cfr–GPI; overlaid, anti-FLAG of FLAG–Cfr–GPI (black), FLAG–CfrΔ16–GPI (red), FLAG–CfrΔ15–16–GPI (blue) and FLAG–CfrΔ13–16–GPI (green). Cell-surface expression of the GPI-anchored Cfr mutants increased as the number of Cfr repeats decreased. (**B**) Western and Northern blot analyses of total protein and mRNA of the deletion mutants. The mutants were clearly detected in the Western blot analysis. (**C**) Immunofluorescent staining of Ba/F3 cells expressing the deletion mutants. In the merged photographs, signals of FLAG (red), TGOLN2 (Tgn46, green) and nuclei (blue) are merged. Scale bar, 20 μm. The FLAG signals on the cell surface were slightly stronger in FLAG–CfrΔ13–16–GPI than FLAG–Cfr–GPI.

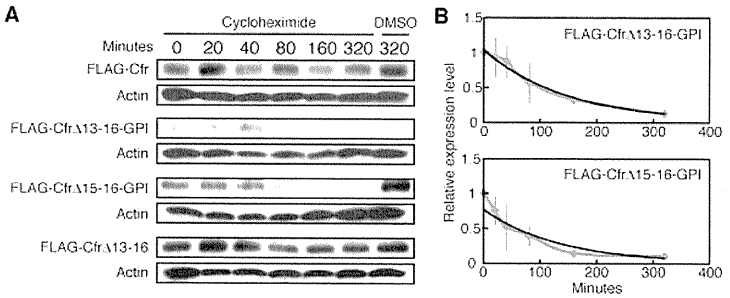

Figure 6 Protein stability assay of the Cfr mutants

(**A**) Ba/F3 cells expressing the Cfr mutants were incubated with 50 μg/ml cycloheximide for the indicated periods, and then harvested for Western blot analysis. As a control the solvent DMSO was added. The GPI-anchored mutants showed decreased stability. By contrast, FLAG–Cfr and FLAG–CfrΔ13–16 was stable and showed no decline in the amount of protein. (**B**) The half-life curves for the GPI-anchored mutants. The results were derived from three independent experiments. The half-lives of FLAG–CfrΔ13–16–GPI and FLAG–CfrΔ15–16–GPI are 102.6 and 92.7 min respectively.

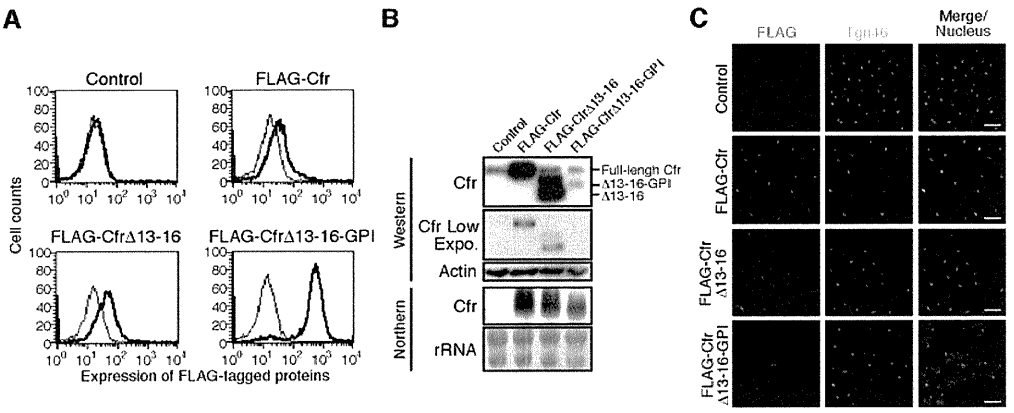

Figure 7 Retention of the Cfr deletion mutant in the Golgi apparatus by the C-terminus of Cfr

(**A**) Flow cytometric analysis of FLAG–CfrΔ13–16. Filled, isotype control; open, anti-FLAG. Deletion of the Cfr repeats did not strongly enhance the cell-surface expression of FLAG–Cfr in the presence of the transmembrane domain and cytoplasmic tail. (**B**) Western and Northern blot analyses of FLAG–CfrΔ13–16 protein and mRNA. The results of low exposure in the Western blot analysis are also shown (Cfr Low Expo.). The amounts of FLAG–Cfr and FLAG–CfrΔ13–16 are comparable. (**C**) Immunofluorescent staining of FLAG–CfrΔ13–16 in Ba/F3 cells. In the merged panels, signals of FLAG (red), TGOLN2 (Tgn46, green) and nuclei (blue) are merged. Scale bar, 20 μm. Unlike FLAG–CfrΔ13–16–GPI, FLAG–CfrΔ13–16 was mostly located in the Golgi apparatus.

Table 1 Summary of intracellular distribution and protein stability of the Cfr mutants

Comparison with FLAG–Cfr–GPI are shown for some of the mutants.

Cfr mutant	Intracellular distribution	Protein stability
FLAG–Cfr	Golgi and weakly cell surface	Very stable
FLAG–CfrΔ1169	Cell surface	Unstable
FLAG–Cfr–GPI	Cell surface	Unstable
FLAG–CfrΔ13–16–GPI	Cell surface (>FLAG–Cfr–GPI)	Stable (>FLAG–Cfr–GPI)
FLAG–CfrΔ15–16–GPI	Cell surface (>FLAG–Cfr–GPI)	Stable (>FLAG–Cfr–GPI)
FLAG–CfrΔ16–GPI	Cell surface (>FLAG–Cfr–GPI)	Stable (>FLAG–Cfr–GPI)
FLAG–Cfr–KARA–GPI	Cell surface (= FLAG–Cfr–GPI)	Unstable (= FLAG–Cfr–GPI)
FLAG–CfrΔ16	Golgi and weakly cell surface	Very stable

indicating that destabilization of Cfr by the Cfr repeats does not occur in the Golgi apparatus (Figure 7C). This possibility was further supported by the stability of FLAG–CfrΔ13–16, which was comparable with that of the full-length Cfr (Figure 6A).

Regulatory mechanisms for the intracellular distribution of Cfr in other cells and proteins

Finally, we addressed whether the regulatory mechanisms for the intracellular distribution of Cfr are general. First, we expressed the Cfr mutants in NIH 3T3 cells to confirm our results in Ba/F3 cells, and found that the mutants were expressed in NIH 3T3 cells with patterns basically the same as those in Ba/F3 cells (Figure 8A). In addition, we also observed that the Cfr mutants were expressed with the same patterns in COS7 cells (results not shown). We have summarized the intracellular distribution and protein stability of the Cfr mutants in Table 1.

Next, we investigated whether the mechanisms work in other proteins. It has been already shown that fusion of the C-terminal region of Cfr to the extracellular domain of CD8 directs the fusion protein to the Golgi apparatus [11]. Therefore we generated a fusion protein of another cell-surface protein EpCAM and the Cfr repeats (EpCAM-CfrRepeat; Figure 8B). We expressed this fusion protein in Ba/F3 cells in parallel with wild-type EpCAM, and monitored their expression on the cell surface by flow cytometry and a biotin-labelling assay. Interestingly, the insertion of the Cfr repeats decreased the surface expression of EpCAM (Figures 8C and 8D). We then monitored mRNA and protein expression of EpCAM–CfrRepeat and found that whereas the amount of mRNA was comparable between EpCAM and EpCAM–CfrRepeat, the amount of EpCAM–CfrRepeat protein was extremely low (Figure 8E). We monitored further the intracellular distribution of EpCAM – CfrRepeat by immunofluorescent staining. EpCAM was expressed strongly on the cell surface, but the strength of the EpCAM–CfrRepeat signal was lower than that of EpCAM (Figure 8F).

These results clearly show that Cfr is at first retained in the Golgi apparatus through its transmembrane domain and cytoplasmic tail, and then subjected to stability control through the Cfr repeats during its recruitment to the plasma membrane or on the cell surface (Figure 8G).

DISCUSSION

Cfr is unique in that it has been identified independently as an Fgf-binding protein, a latent TGFβ-binding protein, a ligand for E-selectin and a protein of the Golgi apparatus [1,4,7,8]. However, its physiological functions had been unknown. Recently, we [3] and Yang et al. [9] independently generated *Cfr*-deficient mice and reported that they show skeletal phenotypes. We reported that Cfr is a positive regulator of the Fgf18 signalling pathway, and revealed in the present study that the interaction between Cfr and Fgf18 on the cell surface is important for Cfr's actions (Figure 2), whereas Yang et al. [9] indicated that it also contributes to TGFβ signalling by binding the precursor of TGFβ in the Golgi apparatus. Furthermore, the function of Cfr as a ligand for E-selectin has been well confirmed by knockdown experiments, although no obvious phenotype in cell adhesion via selectins, such as lymphocyte rolling, has been observed in *Cfr*-deficient mice [16]. Cfr is ubiquitously expressed in almost all cells and tissues from very early in embryonic development to adulthood [3]. Therefore, considering the pleiotropic roles of Fgf and TGFβ signalling in development, the phenotypes of *Cfr*-deficient mice would be much more severe if Cfr functions the same way in all cells. Rather, Cfr seems to perform different roles according to its cellular context. We speculate that a key determinant is its intracellular distribution. When located in the Golgi apparatus,

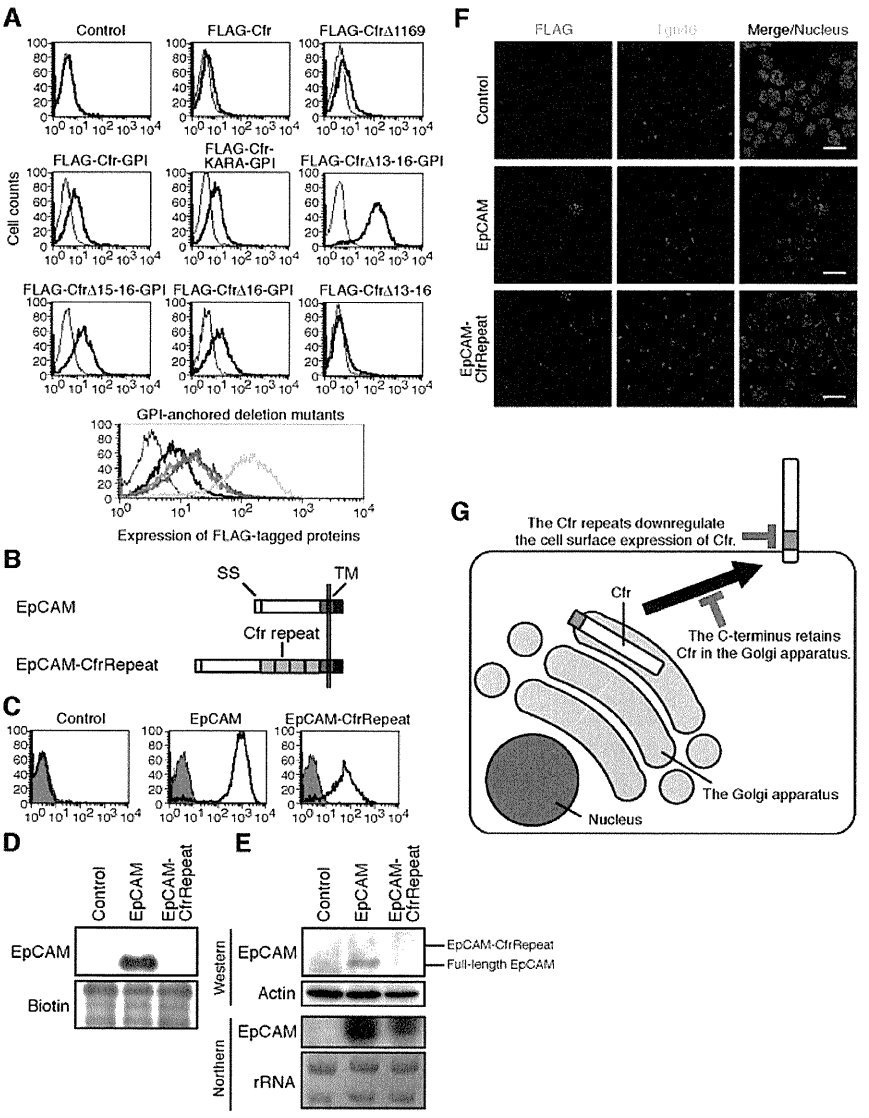

Figure 8 Cell-surface expression of the Cfr mutants in NIH 3T3 cells and destabilization of EpCAM by the Cfr repeats

(**A**) Flow cytometric analysis of the cell-surface expression of the Cfr mutants in NIH 3T3 cells. For each sample: filled, isotype control; open, anti-FLAG. For the panel showing GPI-anchored deletion mutants: filled, isotype control of FLAG–Cfr–GPI; open, anti-FLAG of FLAG–Cfr–GPI (black), FLAG–CfrΔ16–GPI (red), FLAG–CfrΔ15–16–GPI (blue) and FLAG–CfrΔ13–16–GPI (green). (**B**) Schematic representation of EpCAM–CfrRepeat. EpCAM–CfrRepeat has Cfr repeats 13–16 inserted between the extracellular domain and transmemebrane region of EpCAM. SS, signal sequence; TM, transmembrane domain. (**C**) Cell-surface expression of EpCAM and EpCAM–CfrRepeat monitored by flow cytometry. Filled, isotype control; open, anti-EpCAM. (**D**) Cell surface expression of EpCAM and EpCAM-CfrRepeat monitored by biotin-labelling assay. Proteins on the cell surface were biotin-labelled and pulled down. The precipitates were subjected to Western blot analysis for EpCAM. The total amount of biotin-labelled surface protein was monitored by streptavidin (biotin). (**E**) Western and Northern blot analyses of EpCAM and EpCAM–CfrRepeat protein and mRNA. (**F**) Immunofluorescent staining of EpCAM and EpCAM–CfrRepeat in Ba/F3 cells. In the merged panels, signals of EpCAM (red), TGOLN2 (Tgn46, green) and nuclei (blue) are merged. Scale bar, 20 μm. (**G**) A two-step model for regulation of the intracellular distribution of Cfr. First, Cfr is subjected to selection between retention in the Golgi apparatus and transport to the cell surface. The C-terminus of Cfr is involved in this process to retain Cfr in the Golgi apparatus. Secondly, the amount of Cfr on the cell surface is controlled by its stability. With the Cfr repeats, Cfr is destabilized and its cell-surface expression is decreased.

Cfr can act as a regulator of the TGFβ signalling pathway, but it needs to be on the cell surface to function as a regulator of the Fgf signalling pathway or a ligand for E-selectin. We also observed that wild-type Cfr expressed in Ba/F3 cells and NIH 3T3 cells occurred not only in the Golgi apparatus, but also on the cell surface (Figures 1B and 8A), and it has been reported that endogenous Cfr is also expressed on the cell surface in 32Dcl3 cells and neutrophils [17]. Therefore we investigated the mechanisms regulating the intracellular distribution of Cfr.

Previous studies have shown that the cytoplasmic tail is important for the localization of Cfr to the Golgi apparatus in rats and humans [10,11]. We also confirmed that it is required for the retention of Cfr in the Golgi apparatus in mice (Figures 1B and 1C). In addition, we revealed that replacement of the transmembrane and cytoplasmic domains with the GPI anchor signal sequence further enhanced the cell-surface expression (Figures 1B and 1C). From these results, not only the cytoplasmic tail but also the transmembrane domain could contribute to the retention of Cfr in the Golgi apparatus, like many other transmembrane proteins in the Golgi apparatus [18]. Moreover, these C-terminally modified mutants were extremely unstable compared with full-length Cfr, indicating that having left the

Golgi apparatus Cfr is destabilized (Figure 3A). This possibility was further directly confirmed by the protein stability assay. The Cfr mutants that were no longer localized in the Golgi apparatus exhibited much shorter half-lives compared with full-length Cfr (Figure 6). Unexpectedly, this destabilization is not due to the lysosome or proteasome (Figures 3B and 3C). Therefore we searched by mutagenic analysis for regions responsible for the instability.

It has been reported that the extracellular domain of Cfr is cleaved and secreted into the culture supernatant. The molecular mass of the secreted Cfr fragment almost corresponded with that of the extracellular domain, indicating that the cleavage occurs very near the transmembrane domain of Cfr [8,12]. Indeed, we also observed the shed extracellular domain of Cfr in the culture supernatants, but its amount was comparable between FLAG–Cfr and FLAG–Cfr–GPI. These results indicate that the shedding is not a main cause of the instability of Cfr outside the Golgi apparatus. As it was suggested previously that basic amino acid residues in the juxtamembrane region are the targets of the cleavage [8], we examined further the possibility that the cleavage contributes to the instability by making substitutions with an alanine residue. However, the expression of FLAG–Cfr–GPI protein was not affected by the mutations (Figures 4B and 4C). Instead, we found that deletion of the last four Cfr repeats dramatically enhanced the cell-surface expression of FLAG–Cfr–GPI (Figure 5). To find the specific site for the instability, we deleted the last repeat or two repeats from FLAG–Cfr–GPI and found that the surface expression of these GPI-anchored mutants reduced gradually depending on the number of Cfr repeats (Figure 5A). These results suggest that the Cfr repeats rather than a specific sequence for cleavage in the juxtamembrane region are responsible for the instability of Cfr. Interestingly, the repeats also reduced the amount of EpCAM protein when they were inserted in its juxtamembrane region (Figure 8). These results also support that the Cfr repeats function as a general module for protein destabilization.

To examine the function of the Cfr repeat further, we deleted the last four repeats from the full-length Cfr (Figure 1A). However, FLAG–CfrΔ13–16 was still found in the Golgi apparatus, indicating that the presence of the transmembrane domain and cytoplasmic tail is sufficient for the retention of Cfr in the Golgi apparatus (Figures 7A and 7C). Moreover, the stability control via the Cfr repeats does not take place in the Golgi apparatus, because the amount and half-life of FLAG–CfrΔ13-16 were comparable with that of FLAG–Cfr (Figures 6A and 7B). This observation also excludes the possibility that the stability control by the Cfr repeat is due to non-specific effects. These results clearly demonstrate that Cfr is destabilized after passing through the Golgi apparatus.

On the basis of our findings, we propose a two-step model for regulation of the intracellular distribution of Cfr (Figure 8G). First, Cfr is retained via its transmembrane domain and cytoplasmic tail in the Golgi apparatus in a manner similar to that of many other transmembrane proteins. It has been accepted that transmembrane proteins located in the Golgi apparatus have a relatively short transmembrane domain (~15 amino acids) compared with that of the plasma membrane proteins (~20 amino acids). This short transmembrane domain fits the properties of lipids constituting the membrane of the Golgi apparatus and retains proteins with this domain in the Golgi apparatus [19]. However, the transmembrane domain of Cfr is composed of 21 amino acids, indicating that the localization of Cfr in the Golgi apparatus is independent of the length of the transmembrane domain. Furthermore, the tyrosine-based motif in the cytoplasmic domain functions as a retrieval signal from the plasma membrane to the Golgi apparatus in some transmembrane proteins located in the Golgi apparatus such as TGOLN2 [20–22]. However, Cfr has no tyrosine residues in its cytoplasmic tail, indicating that Cfr occurs in the Golgi apparatus by other mechanisms. It has been reported that the transmembrane domains and cytoplasmic regions interact with each other to form a large complex, preventing transport to other destinations (the 'kin recognition' mechanism) [18,23]. This is a possible mechanism regulating the distribution of Cfr. If Cfr is also retained in the Golgi apparatus by 'kin recognition', modification of the transmembrane region and cytoplasmic tail should alter the intracellular localization of Cfr. Secondly, after leaving the Golgi apparatus, Cfr is destabilized via its Cfr repeats in the juxtamembrane region, resulting in reduced cell-surface expression. This step seems to be specific to Cfr, and we speculate that there may be a factor recognizing the Cfr repeats to destabilize Cfr. The fact that EpCAM–CfrRepeat is also further destabilized supports the existence of a *trans*-acting factor on the Cfr repeats (Figure 8). Therefore expression of this factor, or modification of the recognized sites in the Cfr repeat should affect the localization of Cfr. Alternatively, a portion of Cfr may be transported to the surface by simply escaping from this two-step regulation when expressed abundantly. Thus the intracellular distribution of Cfr can be modified at multiple points to direct it into the Golgi apparatus, or on to the cell surface, determining its functions.

AUTHOR CONTRIBUTION

Yuichiro Miyaoka, Hidenori Kato and Kazuki Ebato performed the experiments and analysed the data. Shigeru Saito and Naoko Miyata performed the cell sorting. Toru Imamura contributed the Ba/F3 cell line expressing Fgfr3c and provided advice on experimental design. Yuichiro Miyaoka designed the research project. Yuichiro Miyaoka and Atsushi Miyajima wrote the paper.

ACKNOWLEDGEMENTS

We thank Dr M. Asada and Dr M. Suzuki (National Institute of Advanced Industrial Science and Technology, Tsukuba, Japan) for helpful discussions. We also thank Dr D.M. Ornitz (Washington University, St Louis, MO, U.S.A.) and Dr Y. Yamazumi (The University of Tokyo, Tokyo, Japan) for providing cDNA for Fgfrs and human cDNA respectively.

FUNDING

This work was supported, in part, by a Grant-in-Aid for Young Scientists [grant number 22791363 (to Y.M.)] and a Grant-in-Aid for Scientific Research to A.M. from the Ministry of Education, Science and Culture, Japan and the Takeda Science Foundation.

REFERENCES

1 Burrus, L. W. and Olwin, B. B. (1989) Isolation of a receptor for acidic and basic fibroblast growth factor from embryonic chick. J. Biol. Chem. **264**, 18647–18653
2 Zhou, Z., Zuber, M. E., Burrus, L. W. and Olwin, B. B. (1997) Identification and characterization of a fibroblast growth factor (FGF) binding domain in the cysteine-rich FGF receptor. J. Biol. Chem. **272**, 5167–5174
3 Miyaoka, Y., Tanaka, M., Imamura, T., Takada, S. and Miyajima, A. (2010) A novel regulatory mechanism for Fgf18 signaling involving cysteine-rich FGF receptor (Cfr) and delta-like protein (Dlk). Development **137**, 159–167
4 Gonatas, J. O., Mezitis, S. G., Stieber, A., Fleischer, B. and Gonatas, N. K. (1989) MG-160. A novel sialoglycoprotein of the medial cisternae of the Golgi apparatus. J. Biol. Chem. **264**, 646–653
5 Croul, S., Mezitis, S. G., Stieber, A., Chen, Y. J., Gonatas, J. O., Goud, B. and Gonatas, N. K. (1990) Immunocytochemical visualization of the Golgi apparatus in several species, including human, and tissues with an antiserum against MG-160, a sialoglycoprotein of rat Golgi apparatus. J. Histochem. Cytochem. **38**, 957–963
6 Stieber, A., Mourelatos, Z., Chen, Y. J., Le Douarin, N. and Gonatas, N. K. (1995) MG160, a membrane protein of the Golgi apparatus which is homologous to a fibroblast growth factor receptor and to a ligand for E-selectin, is found only in the Golgi apparatus and appears early in chicken embryo development. Exp. Cell Res. **219**, 562–570

7 Steegmaier, M., Levinovitz, A., Isenmann, S., Borges, E., Lenter, M., Kocher, H. P., Kleuser, B. and Vestweber, D. (1995) The E-selectin-ligand ESL-1 is a variant of a receptor for fibroblast growth factor. Nature **373**, 615–620
8 Olofsson, A., Hellman, U., Ten Dijke, P., Grimsby, S., Ichijo, H., Moren, A., Miyazono, K. and Heldin, C. H. (1997) Latent transforming growth factor-β complex in Chinese hamster ovary cells contains the multifunctional cysteine-rich fibroblast growth factor receptor, also termed E-selectin-ligand or MG-160. Biochem J. **324**, 427–434
9 Yang, T., Mendoza-Londono, R., Lu, H., Tao, J., Li, K., Keller, B., Jiang, M. M., Shah, R., Chen, Y., Bertin, T. K. et al. (2010) E-selectin ligand-1 regulates growth plate homeostasis in mice by inhibiting the intracellular processing and secretion of mature TGF-β. J. Clin. Invest. **120**, 2474–2485
10 Gonatas, J. O., Chen, Y. J., Stieber, A., Mourelatos, Z. and Gonatas, N. K. (1998) Truncations of the C-terminal cytoplasmic domain of MG160, a medial Golgi sialoglycoprotein, result in its partial transport to the plasma membrane and filopodia. J. Cell Sci. **111**, 249–260
11 Ahn, J., Febbraio, M. and Silverstein, R. L. (2005) A novel isoform of human Golgi complex-localized glycoprotein-1 (also known as E-selectin ligand-1, MG-160 and cysteine-rich fibroblast growth factor receptor) targets differential subcellular localization. J. Cell Sci. **118**, 1725–1731
12 Antoine, M., Kohl, R., Tag, C. G., Gressner, A. M., Hellerbrand, C. and Kiefer, P. (2009) Secreted cysteine-rich FGF receptor derives from post-translational processing by furin-like prohormone convertases. Biochem. Biophys. Res. Commun. **382**, 359–364
13 Notohamiprodjo, M., Djafarzadeh, R., Mojaat, A., von Luttichau, I., Grone, H. J. and Nelson, P. J. (2006) Generation of GPI-linked CCL5 based chemokine receptor antagonists for the suppression of acute vascular damage during allograft transplantation. Protein Eng. Des. Sel. **19**, 27–35
14 Okabe, M., Tsukahara, Y., Tanaka, M., Suzuki, K., Saito, S., Kamiya, Y., Tsujimura, T., Nakamura, K. and Miyajima, A. (2009) Potential hepatic stem cells reside in EpCAM + cells of normal and injured mouse liver. Development **136**, 1951–1960
15 Miyaoka, Y., Tanaka, M., Naiki, T. and Miyajima, A. (2006) Oncostatin M inhibits adipogenesis through the RAS/ERK and STAT5 signaling pathways. J. Biol. Chem. **281**, 37913–37920
16 Hidalgo, A., Peired, A. J., Wild, M. K., Vestweber, D. and Frenette, P. S. (2007) Complete identification of E-selectin ligands on neutrophils reveals distinct functions of PSGL-1, ESL-1, and CD44. Immunity **26**, 477–489
17 Steegmaier, M., Borges, E., Berger, J., Schwarz, H. and Vestweber, D. (1997) The E-selectin-ligand ESL-1 is located in the Golgi as well as on microvilli on the cell surface. J. Cell Sci. **110**, 687–694
18 Gleeson, P. A. (1998) Targeting of proteins to the Golgi apparatus. Histochem. Cell Biol. **109**, 517–532
19 Bretscher, M. S. and Munro, S. (1993) Cholesterol and the Golgi apparatus. Science **261**, 1280–1281
20 Bos, K., Wraight, C. and Stanley, K. K. (1993) TGN38 is maintained in the *trans*-Golgi network by a tyrosine-containing motif in the cytoplasmic domain. EMBO J. **12**, 2219–2228
21 Humphrey, J. S., Peters, P. J., Yuan, L. C. and Bonifacino, J. S. (1993) Localization of TGN38 to the *trans*-Golgi network: involvement of a cytoplasmic tyrosine-containing sequence. J. Cell Biol. **120**, 1123–1135
22 Ponnambalam, S., Rabouille, C., Luzio, J. P., Nilsson, T. and Warren, G. (1994) The TGN38 glycoprotein contains two non-overlapping signals that mediate localization to the *trans*-Golgi network. J. Cell Biol. **125**, 253–268
23 Chen, W. and Stanley, P. (2003) Five Lec1 CHO cell mutants have distinct *Mgat1* gene mutations that encode truncated *N*-acetylglucosaminyltransferase I. Glycobiology **13**, 43–50

Received 18 February 2011/11 July 2011; accepted 21 July 2011
Published as BJ Immediate Publication 21 July 2011, doi:10.1042/BJ20110318

Chapter 3

Identification and Isolation of Adult Liver Stem/Progenitor Cells

Minoru Tanaka and Atsushi Miyajima

Abstract

Hepatoblasts are considered to be liver stem/progenitor cells in the fetus because they propagate and differentiate into two types of liver epithelial cells, hepatocytes and cholangiocytes. In adults, oval cells that emerge in severely injured liver are considered facultative hepatic stem/progenitor cells. However, the nature of oval cells has remained unclear for some time due to the lack of a method to isolate them. It has also been unclear whether liver stem/progenitor cells exist in normal adult liver. Recently, we and others have successfully identified oval cells and adult liver stem/progenitor cells. Here, we describe the identification and isolation of mouse liver stem/progenitor cells by utilizing antibodies against specific cell surface marker molecules.

Key words: Liver stem/progenitor cells, Oval cells, Flow cytometry, Antibody

1. Introduction

The adult liver has a remarkable potential to regenerate when injured. In many cases, hepatocytes replicate to repair the damage (1, 2). However, if the injury limits the proliferation of hepatocytes, facultative progenitor cells proliferate around portal veins; this is known as a ductal reaction (3, 4). These proliferating epithelial cells, often referred to as "oval cells" in rodents, are believed to contribute to liver regeneration (5). The nature of oval cells as liver stem cells has been debated based on numerous studies using various rodent models. In mice, a diet containing 3,5-diethoxycarbonyl-1,4-dihydro-collidine (DDC) and a choline-deficient, ethionine-supplemented (CDE) diet have been developed to induce oval cell activation (6–8). Although these proliferating epithelial cells upon

Takahiro Ochiya (ed.), *Liver Stem Cells: Methods and Protocols*, Methods in Molecular Biology, vol. 826,
DOI 10.1007/978-1-61779-468-1_3, © Springer Science+Business Media, LLC 2012

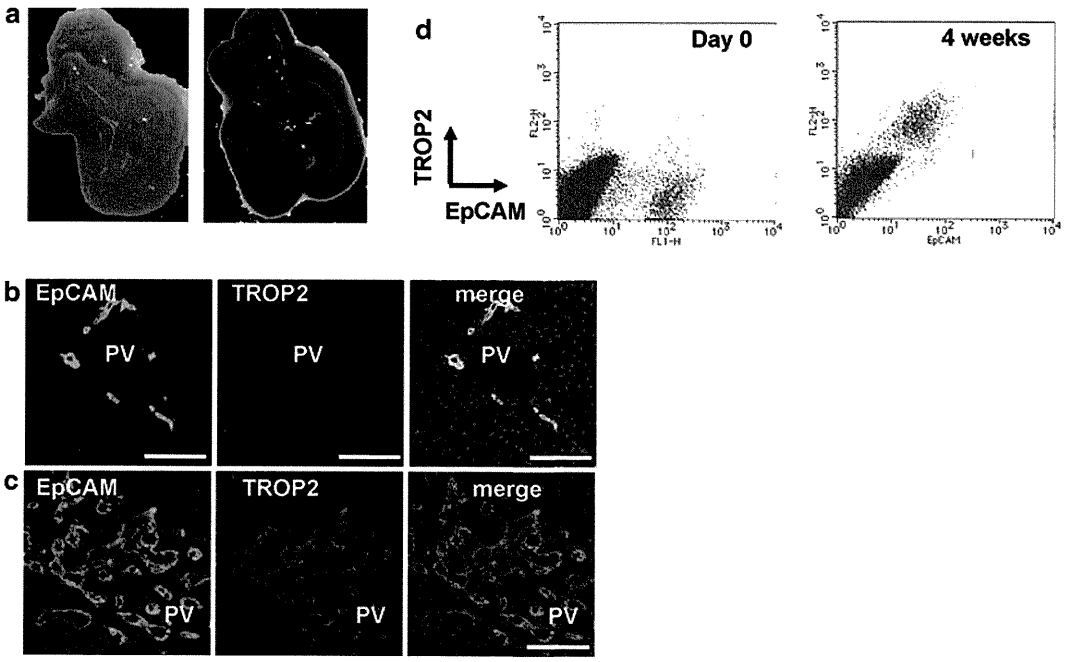

Fig. 1. The DDC-containing diet causes hepatic injury and oval cell activation. (**a**) Appearance of normal liver (*left panel*) and liver damaged by DDC (*right panel*). (**b**, **c**) Immunohistochemistry of frozen sections of normal liver (**b**) and the liver of mice fed DDC for 5 weeks (**c**) with anti-EpCAM and anti-TROP2 Abs. TROP2 is expressed in oval cells but not in normal cholangiocytes. (**d**) Flow cytometric analysis of nonparenchymal cells with anti-EpCAM and anti-TROP2 Abs after DDC feeding. *PV* portal vein. Scale bar, 100 μm.

injury by various insults are collectively referred to as oval cells, it remains unclear whether or not those cells in different species by different protocols have common characteristics. To address this issue, oval cells need to be precisely identified and isolated for clonal analysis. Recently, we and others have identified and characterized adult liver stem/progenitor cells by utilizing cell surface markers (9–13). We identified TROP2 and epithelial cell adhesion molecule (EpCAM) as markers expressed in oval cells (Fig. 1) and by using antibodies, isolated the oval cell compartment from the injured livers of mice fed a diet containing DDC. Furthermore, we developed culture system and characterized EpCAM+ cells isolated from normal as well as injured livers. Here, we describe the methods for identifying and isolating mouse liver stem/progenitor cells.

2. Materials

2.1. Generation of Oval Cells in Mouse Liver

1. Adult male mice (8–12 weeks old). C57BL/6 mice were used for all experiments.
2. Diet containing 0.1% DDC (Bio-Serv).

2.2. Immunohistochemistry of Frozen Liver Sections by Zamboni's Fixation (A Modified Paraformaldehyde-Based Fixation Method)

1. Solution A: Saturated Picric acid solution in distilled water available commercially from Sigma-Aldrich, etc. Any solid materials were removed by filtration before use.
2. Solution B: Twenty grams of paraformaldehyde were dissolved in 100 mL of distilled water. The solution was warmed to 60°C and stirred to melt the paraformaldehyde. A small amount of 1 N NaOH was added if necessary. After complete dissolution, the solution was cooled down. If necessary, it was filtrated.
3. Zamboni's solution: 150 mL of solution A and 100 mL of solution B were mixed well, and 750 mL of PBS (pH 7.4) added to adjust the total volume to 1 L. This solution can be stored at 4°C for at least 1 year.

2.3. Isolation of EpCAM+ Cells from Livers of Normal and DDC Diet-Fed Mice

[AU1]

1. Perfusion solution I: Liver Perfusion Medium (GIBCO 17701-038).
2. Perfusion solution II: 8 g NaCl, 0.4 g KCl, 0.56 g $CaCl_2$, 0.078 g $NaH_2PO_4 \cdot 2H_2O$, 0.151 g $Na_2HPO_4 \cdot 12H_2O$, 0.9 g glucose, 0.35 g $NaHCO_3$, and 2.38 g HEPES were dissolved in distilled and deionized water [made up to 1 L and filtered through a 0.22-μm STERICUP (Millipore)].
3. Collagenase solution I: 50 mg of collagenase (Sigma C-5138), 25 mg of DNaseI (Sigma DN25-1G), and 10 mL of FBS were added to 90 mL of perfusion solution II, mixed well, and filtered through a 0.22-μm STERICUP (Millipore) (made fresh as required) (see Note 1).
4. Collagenase solution II: 50 mg of pronase (Roche) was dissolved in 100 mL of Collagenase solution I, mixed well, and filtered through a 0.22-μm STERICUP (Millipore) (made fresh as required).
5. Washing solution: William's E medium containing 10% FBS.
6. Hemolysis buffer: 1 g of Trizma base (Sigma) and 2.8 g of NH_4Cl were dissolved in 500 mL of distilled and deionized water.
7. Catheter of 24 G×3/4" indwelling needle (TERUMO, SR-OT2419C).
8. Peristaltic pump: Masterflex L/S Variable-Speed Modular Drives (HV-07553-80) with silicone tubing (HV-96410-13) (Cole-Parmer, IL).
9. Antibodies: Biotinylated goat anti-TROP2 antibody (BAF1122) (R&D Systems), rat anti-EpCAM antibody (Clone G8.8) (BioLegend) or (Clone 2-17) (MBL International), and FcBlock (BD).

2.4. Culture of EpCAM+ Cells Isolated from Normal and DDC Diet-Fed Liver

1. Standard medium: Williams' medium E containing 10% FBS, 10 mM nicotinamide, 2 mM L-glutamine, 0.2 mM ascorbic acid, 20 mM HEPES pH 7.5, 1 mM sodium pyruvate, 17.6 mM $NaHCO_3$, 14 mM glucose, 100 nM dexamethasone,

1× ITS (insulin, transferrin, selenium X) (GIBCO) and 50 μg/mL gentamicin.

2. Cytokines: Human EGF and human recombinant HGF (final concentration of 10 ng/mL each).
3. Type-I collagen-coated dish: 35 mm dishes were coated with Type-I collagen solution (Cellmatrix Type I-C, Nitta gelatin).
4. Trypsin: 0.25% Trypsin–EDTA (#25200)(GIBCO).

3. Methods

3.1. Generation of Oval Cells and Immunohistochemistry

1. Mice were fed by the DDC-containing diet for more than 4 weeks (see Note 2). After sacrifice, the whole livers were removed carefully, dissected into pieces of 5 mm and fixed by incubation in Zamboni's solution at 4°C for 8 h to O/N (see Note 3).
2. The fixed tissues were immersed in 10% sucrose/PBS, 15% sucrose/PBS, and 20% sucrose/PBS for 1 day each. Then, the tissues were frozen in OCT compound. Sections (8 μm) were prepared with a cryostat and incubated with each antibody, followed by a fluorescein-conjugated secondary antibody (see Note 4).

3.2. Isolation of EpCAM+ Cells from Mouse Liver

1. Liver perfusion solution I (20 mL per a mouse) and collagenase solution I (25 mL per mouse) were warmed at 37°C in a water bath, and a 50-mL glass beaker containing collagenase solution II (10 mL per mouse) was placed in an air incubator at 37°C.
2. An anesthetized mouse was fixed on a cork board and 70% ethanol sprayed on the abdominal skin. The abdomen was opened and the intestine moved over to the right side (Fig. 2a). The portal vein was cut with surgical scissors without broken away. The bleeding was absorbed with cotton gauze to prevent blood from pooling (Fig. 2b). The hole was cannulated with a catheter connected to a peristaltic pump (Fig. 2c) (see Note 5). Perfusion solution I was delivered at a speed of 3 mL/min (Fig. 2d) and then the vena cava inferior was cut (Fig. 2e). After perfusion for 5 min (total volume, approximately 15 mL) (Fig. 2f), perfusion solution I was replaced with collagenase solution I and the perfusion continued for 8 min (total volume, approximately 25 mL).
3. After digestion, the whole liver was carefully removed and transferred to a Petri dish (10 cm in diameter) (see Note 6). 20 mL of washing solution was added to the dish and the liver capsule was torn by crossing two pairs of fine tweezers.

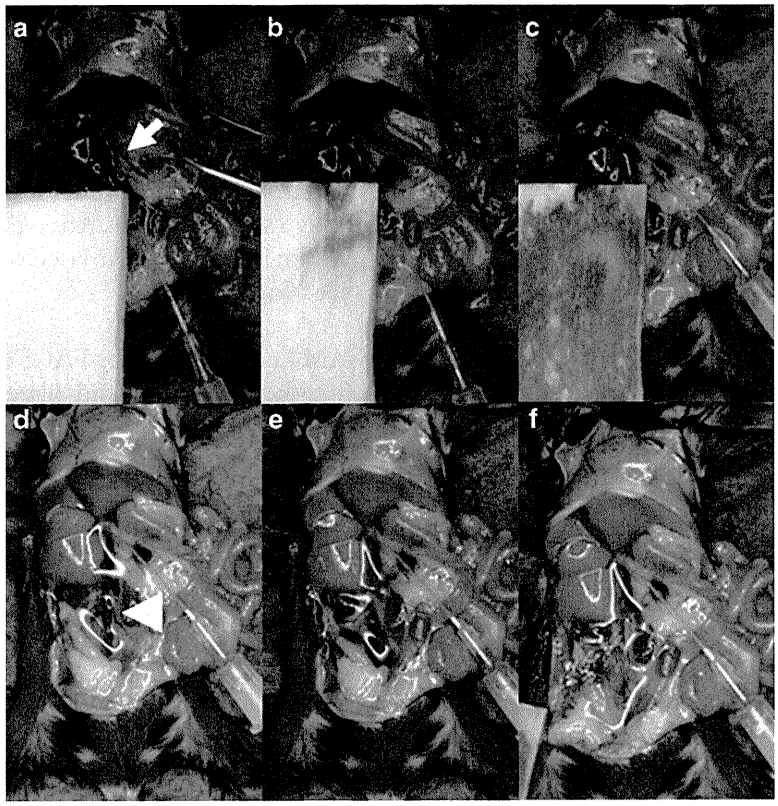

Arrow; portal vein, arrowhead; vena cava

[AU2] Fig. 2. Cannulation of mouse liver.

The contents of the liver were dispersed in the solution and pipetted up and down actively until no lumps remained (see Note 7). Then, the cell suspension was passed through a 70-μm filter to remove undigested clots, including the biliary tree and the filtrate was kept on ice (Cell Suspension A). The residual mass on the filter was transferred to prewarmed collagenase solution II and stirred on a magnetic stirrer for 20 min at 37°C in an air incubator. After digestion, it was pipetted up and down and filtered as previously explained (Cell Suspension B).

4. Cell Suspension A and Cell Suspension B were mixed in a 50 mL disposable tube and washing solution was added to make a total volume of 50 mL. The solution was centrifuged at approximately $100 \times g$ for 2 min to remove parenchymal cells (hepatocytes). The supernatant was transferred to another fresh tube and the centrifugation was repeated twice (see Note 8).
5. After centrifugation of the supernatant at $300 \times g$ for 5 min, the pellet was suspended with 7 mL of hemolysis buffer and kept on ice for 3 min. Then, 8 mL of washing solution was added and centrifuged at $300 \times g$ for 5 min. The pellet was resuspended

with 10 mL of 3% FBS/PBS and filtered with 70 μm mesh to remove debris (see Note 9).

6. After centrifugation at 300×*g* for 5 min, the pellet was resuspended in 300–500 μL of 3% FBS/PBS. Nonspecific binding was blocked by incubating with FcBlock, and the cell suspension was incubated with fluorescein-conjugated anti-EpCAM antibody (see Note 10). After the staining of dead cells with propidium iodide, EpCAM+ cells were sorted by FACSVantage SE (see Note 11).

3.3. Culture of EpCAM+ Cells Isolated from Normal and DDC Diet-Fed Liver

1. EpCAM+ cells isolated by FACSVantage SE were suspended in the Standard Medium and plated at 1×10^4 cells per Type-I collagen-coated 35-mm dish. Human EGF and human recombinant HGF were added to the culture to a final concentration of 10 ng/mL each.
2. After 9 days of culture, the proliferating cells were trypsinized, washed, and replated onto new culture dishes (Fig. 3) (see Note 12). They continued to grow even after serial passages for more than 6 months, and possessed the potential to differentiate into hepatocytic and cholangiocytic cell lineages under the adequate culture conditions (12).

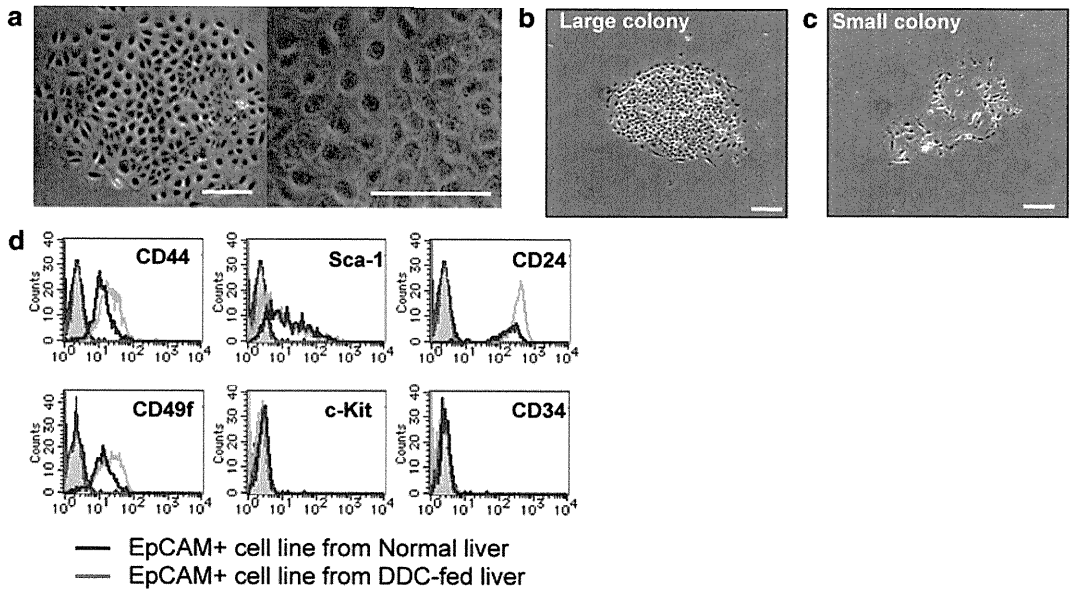

Fig. 3. Characteristics of proliferative EpCAM+ cells. (**a**) Morphology of proliferative cells with characteristic of liver stem cells derived from EpCAM+ cells of DDC diet-fed livers. (**b**, **c**) Appearance of a large colony (**b**) with the potential to proliferate, and a small colony (**c**) with limited growth derived from EpCAM+ cells of normal livers. (**d**) Flow cytometric analysis of some cell surface markers in established cell lines with characteristics of liver stem cells. The cells derived from normal (*blue line*) and DDC diet-fed (*red line*) livers show similar expression profiles of cell surface markers. Scale bar: 200 μm.

4. Notes

1. Chronic hepatitis induced by the administration of DDC often makes the liver fibrotic. We recommend this collagenase for efficient digestion of the fibrotic liver. Aliquots of collagenase powder were stored at −80°C until used. Avoid freezing and thawing to maintain the enzymatic activity.
2. The formation of oval cells reaches a plateau at about 4 weeks after the administration of DDC. Prolonged administration for more than 8 weeks may cause death.
3. We strongly recommend Zamboni's solution for the detection of TROP2 because the signal is very faint with other reagents, such as 4% PFA and cold acetone.
4. We usually incubated frozen sections with the first antibody solution (1/50–100 dilution with 5% skim milk/PBS) at 4°C for O/N. We used goat anti-TROP2 antibody (BAF1122) (R&D Systems) and rat anti-EpCAM antibody (Clone G8.8) for immunostaining.
5. We usually cannulated with running solution at a very low speed. Put the catheter toward the bleeding portal vein. Do not insert the catheter too deep into the liver or you will damage a vein. If the perfusion is successfully performed, the liver turns yellowish due to blood removal as shown in Fig. 2d.
6. We usually removed the gall bladder carefully without burst because the bile is toxic.
7. We prefer to use a glass pipette with a latex nipple. This permits vigorous pipetting to disperse the clump of tissues rather than electrical pipettes.
8. Repeat this step until the cell pellet is completely dissolved.
9. Insoluble debris should be removed by filtration to proceed to the flow cytometric analysis.
10. We usually use FTIC-conjugated rat anti-EpCAM antibody (Clone 2–17).
11. We recommend a magnetic bead-based cell separation system to enrich EpCAM+ cells before purification by flow cytometry. We usually use the autoMACS system with anti-FITC microbeads before cell sorting by FACSVantage, which saves time for cell sorting and avoids reducing the viability of EpCAM+ cells.
12. The primary culture contains both small and large colonies at this point. The proliferative cells with characteristics of liver stem/progenitor cells are selectively expanded by serial passages.

References

1. Michalopoulos, G. K. (2010) Liver regeneration after partial hepatectomy: critical analysis of mechanistic dilemmas. *Am J Pathol* **176**, 2–13.
2. Overturf, K., al-Dhalimy, M., Ou, C. N., Finegold, M. and Grompe, M. (1997) Serial transplantation reveals the stem-cell-like regenerative potential of adult mouse hepatocytes. *Am J Pathol* **151**, 1273–1280.
3. Alison, M. R., Golding, M., Sarraf, C. E., Edwards, R. J. and Lalani, E. N. (1996) Liver damage in the rat induces hepatocyte stem cells from biliary epithelial cells. *Gastroenterology* **110**, 1182–1190.
4. Theise, N. D., Saxena, R., Portmann, B. C., Thung, S. N., Yee, H., Chiriboga, L., et al. (1999) The canals of Hering and hepatic stem cells in humans. *Hepatology* **30**, 1425–1433.
5. Farber, E. (1956) Similarities in the sequence of early histological changes induced in the liver of the rat by ethionine, 2-acetylaminofluorene, and 3'-methyl-4-dimethylaminoazobenzene. *Cancer Res* **16**, 142–148.
6. Akhurst, B., Croager, E. J., Farley-Roche, C. A., Ong, J. K., Dumble, M. L., Knight, B., et al. (2001) A modified choline-deficient, ethionine-supplemented diet protocol effectively induces oval cells in mouse liver. *Hepatology* **34**, 519–522.
7. Preisegger, K. H., Factor, V. M., Fuchsbichler, A., Stumptner, C., Denk, H. and Thorgeirsson, S. S. (1999) Atypical ductular proliferation and its inhibition by transforming growth factor beta1 in the 3,5-diethoxycarbonyl-1,4-dihydrocollidine mouse model for chronic alcoholic liver disease. *Lab Invest* **79**, 103–109.
8. Wang, X., Foster, M., Al-Dhalimy, M., Lagasse, E., Finegold, M. and Grompe, M. (2003) The origin and liver repopulating capacity of murine oval cells. *Proc Natl Acad Sci U S A* 100 Suppl 1, 11881–11888.
9. Schmelzer, E., Zhang, L., Bruce, A., Wauthier, E., Ludlow, J., Yao, H. L., et al. (2007) Human hepatic stem cells from fetal and postnatal donors. *J Exp Med* **204**, 1973–1987.
10. Yovchev, M. I., Grozdanov, P. N., Zhou, H., Racherla, H., Guha, C. and Dabeva, M. D. (2008) Identification of adult hepatic progenitor cells capable of repopulating injured rat liver. *Hepatology* **47**, 636–647.
11. Suzuki, A., Sekiya, S., Onishi, M., Oshima, N., Kiyonari, H., Nakauchi, H., et al. (2008) Flow cytometric isolation and clonal identification of self-renewing bipotent hepatic progenitor cells in adult mouse liver. *Hepatology* **48**, 1964–1978.
12. Okabe, M., Tsukahara, Y., Tanaka, M., Suzuki, K., Saito, S., Kamiya, Y., et al. (2009) Potential hepatic stem cells reside in EpCAM+ cells of normal and injured mouse liver. *Development* **136**, 1951–1960.
13. Kamiya, A., Kakinuma, S., Yamazaki, Y. and Nakauchi, H. (2009) Enrichment and clonal culture of progenitor cells during mouse postnatal liver development in mice. *Gastroenterology* **137**, 1114–1126, 1126 e1–14.

OPEN ACCESS Freely available online

PLoS one

TROP2 Expressed in the Trunk of the Ureteric Duct Regulates Branching Morphogenesis during Kidney Development

Yuko Tsukahara, Minoru Tanaka*, Atsushi Miyajima*

Institute of Molecular and Cellular Biosciences, The University of Tokyo, Tokyo, Japan

Abstract

TROP2, a cell surface protein structurally related to EpCAM, is expressed in various carcinomas, though its function remains largely unknown. We examined the expression of TROP2 and EpCAM in fetal mouse tissues, and found distinct patterns in the ureteric bud of the fetal kidney, which forms a tree-like structure. The tip cells in the ureteric bud proliferate to form branches, whereas the trunk cells differentiate to form a polarized ductal structure. EpCAM was expressed throughout the ureteric bud, whereas TROP2 expression was strongest at the trunk but diminished towards the tips, indicating the distinct cell populations in the ureteric bud. The cells highly expressing TROP2 (TROP2^{high}) were negative for Ki67, a proliferating cell marker, and TROP2 and collagen-I were co-localized to the basal membrane of the trunk cells. TROP2^{high} cells isolated from the fetal kidney failed to attach and spread on collagen-coated plates. Using MDCK cells, a well-established model for studying the branching morphogenesis of the ureteric bud, TROP2 was shown to inhibit cell spreading and motility on collagen-coated plates, and also branching in collagen-gel cultures, which mimic the ureteric bud's microenvironment. These results together suggest that TROP2 modulates the interaction between the cells and matrix and regulates the formation of the ureteric duct by suppressing branching from the trunk during kidney development.

Citation: Tsukahara Y, Tanaka M, Miyajima A (2011) TROP2 Expressed in the Trunk of the Ureteric Duct Regulates Branching Morphogenesis during Kidney Development. PLoS ONE 6(12): e28607. doi:10.1371/journal.pone.0028607

Editor: Tsutomu Kume, Feinberg Cardiovascular Research Institute, Northwestern University, United States of America

Received August 1, 2011; **Accepted** November 11, 2011; **Published** December 14, 2011

Funding: This work was supported by research grants from the Ministry of Education, Culture, Sports, Science and Technology of Japan, Ministry of Health, Labour and Welfare of Japan, the Core Research for Evolutional Science and Technology (CREST) program from the Japan Science and Technology Agency and Takeda Science Foundation. The funders had no role in study design, data collection and analysis, decision to publish, or preparation of the manuscript.

Competing Interests: The authors have declared that no competing interests exist.

* E-mail: tanaka@iam.u-tokyo.ac.jp (MT); miyajima@iam.u-tokyo.ac.jp (AM)

Introduction

TROP2, also known as EGP-1, M1S1, GA733-1, and TACSTD2, is a 36-kDa membrane glycoprotein, initially identified as a tumor-associated calcium signal transducer (TACSTD) expressed in gastrointestinal, bladder, lung, and cervix carcinomas and later found to be highly expressed in many other tumors including pancreatic cancers and squamous cell carcinomas of the oral cavity [1]. TROP2 is strongly expressed in trophoblasts forming the outer layer of the blastocyst which develops into the placenta [2]. In the prostate, TROP2 is specifically expressed in prostate stem cells located in the basal region [3]. We have recently found that TROP2 is expressed in hepatic progenitor cells known as oval cells, which are produced in response to severe liver injury and form duct-like structures surrounding the portal vein [4].

TROP2 is structurally related to epithelial cell adhesion molecule (EpCAM), also known as TACSTD1. Both TROP2 and EpCAM are type I transmembrane proteins, consisting of a hydrophobic leader peptide, a thyroglobulin-like domain, a single transmembrane domain and a short cytoplasmic domain. The cytoplasmic tail of TROP2, but not EpCAM, contains a region homologous to phosphatidylinositol 4,5-bisphosphate (PIP2)-binding motif [5]. EpCAM is widely expressed in epithelial cells and plays roles in cell-cell adhesion, cell proliferation and cell motility [6–10]. On the other hand, TROP2 was suggested to enhance the proliferation of tumor cells in an anchorage-independent manner [11] and the formation of tight junctions by interacting with Claudin-1 and -7 in the corneal epithelium [12]. However, TROP2 expression in normal tissues and its functions still remain largely unstudied.

In the development of the mammalian kidney, the ureteric bud epithelium proliferates and branches to form a tree-like structure [13,14]. This process is known as branching morphogenesis and depends on interactions of the ureteric bud with the metanephric mesenchyme and also components of the extracellular matrix (ECM). Factors secreted from the metanephric mesenchyme enhance the proliferation, elongation and branching of the ureteric bud cells, resulting in differentiation to form the collecting duct system. On the other hand, ECM components around the ureteric bud modulate growth factor signaling and provide an anchorage for cell migration via the ECM-specific integrin receptors on the ureteric bud cells [15,16].

The cells forming the tip and trunk of the ureteric bud exhibit different characteristics [17]. The tip cells are proliferating immature cells that are located at the branching points and interact with the metanephric mesenchyme. By contrast, the trunk cells are differentiating into the collecting duct with a rigid structure consisting of polarized epithelial cells. While the molecular mechanisms underlying the establishment of the tip structure have been well studied, little is known about the mechanisms of trunk morphogenesis. In particular, the factors

linking trunk cells to the extracellular environment remain totally unknown.

To gain insights into the functions of TROP2, we examined the expression of TROP2 together with EpCAM during mouse development and found that the two differ significantly. During development, EpCAM was widely expressed in epithelial tissues, whereas TROP2 expression was restricted to EpCAM$^+$ cells in a few organs. In particular, a unique pattern of TROP2 expression was found in fetal kidney, i.e., TROP2 expression increases from the tip toward the trunk of the ureteric bud, whereas EpCAM was expressed uniformly. In this study, we show that the expression pattern does not appear to correlate with the known functions of TROP2 in cell proliferation and tight junction formation. Using anti-TROP2 and anti-EpCAM antibodies (Abs), we isolated the tip cells and trunk cells of the ureteric buds, and revealed that their morphology on collagen-gel differs significantly, i.e. tip cells spread, whereas trunk cells remain a rounded shape. We further demonstrate that TROP2 alters cell shape and motility on collagen-gel using a primary culture of ureteric bud cells and that it also inhibits branching of MDCK cells. Our findings suggest that TROP2 plays a role in the development of a ductal structure of ureteric trunks by suppressing the formation of new branches.

Results

Expression of TROP2 during kidney development

We performed an immunohistochemical analysis of mouse embryos by using anti-EpCAM and anti-TROP2 Abs. At embryonic day 14.5 (E14.5), EpCAM was expressed in a variety of epithelial tissues including lung, gut, kidney, pancreas and epidermis. By contrast, TROP2 expression was restricted to a few tissues including kidney, gut and epidermis, and the TROP2$^+$ cells were a subpopulation of EpCAM$^+$ cells (Fig. 1A–C). Because TROP2 was highly expressed in the kidney, we focused on the expression and role of TROP2 in kidney development.

In mice, the ureteric bud emerges at E10.5 from the Wolffian duct, which is induced by GDNF from metanephric mesenchyme [18,19]. Subsequently, the ureteric buds are also induced to form the first branch at E11.5 and undergo further branching until E14.5~15.0 by the signals from metanephric mesenchyme. Immunostaining in the fetal kidney at E11.5 revealed that EpCAM was uniformly expressed in the ureteric bud and the Wolffian duct (Figure 2A, arrow and arrowhead, respectively) [20]. Interestingly, TROP2 was expressed at the trunk of the ureteric bud and the Wolffian duct, but its expression was weak at the tip of the ureteric bud that is surrounded by metanephric mesenchyme (Figure 2A, yellow arrowhead). At E14.5, although EpCAM was expressed uniformly throughout the ureteric buds, TROP2 was expressed at the trunk but barely detectable at the tip (Figure 2B, yellow arrowhead). This gradient of TROP2 expression at the ureteric bud suggests TROP2 to be involved in morphogenesis of the ureteric bud, especially in the trunk.

Characterization of TROP2$^+$ and EpCAM$^+$ cells in fetal kidney

To characterize the cells expressing TROP2 in the ureteric bud, we performed a flow cytometric analysis and revealed that EpCAM$^+$ cells in E12.5 kidney were divided into at least 2 populations, TROP2$^+$ and TROP2$^-$ cells (Figure 2C). At E14.5, TROP2 expression was up-regulated, resulting in a broad distribution of TROP2 expression from TROP2^{low} to TROP2^{high}. In addition, the EpCAM$^+$TROP2$^-$ cells increased during development, which is consistent with the results of immunostaining. These results suggested that the expression profiles of EpCAM and TROP2 define the distinct cell types in the developing urinary duct. To characterize E14.5 kidney cells, EpCAM$^+$ cells were fractionated into three populations by cell sorting, EpCAM$^+$TROP2$^-$, EpCAM$^+$TROP2^{low} and EpCAM$^+$TROP2^{high} cells, based on the expression levels of TROP2 (Figure 2D).

The tip and trunk cells of the ureteric bud can be distinguished by the expression of specific markers. Quantitative RT-PCR revealed that Ret, Wnt11 and GFRα, tip cell markers [21–24], were highly expressed in EpCAM$^+$TROP2^{low} cells, whereas Wnt9b, a trunk cell marker [25], was strongly expressed in EpCAM$^+$TROP2^{high} cells (Figure 2E). These results indicate that the EpCAM$^+$TROP2^{low} and EpCAM$^+$TROP2^{high} populations include the tip and trunk cells, respectively, and that ureteric bud cells at different locations can be isolated by cell sorting based on TROP2 expression. It has been reported that EpCAM is expressed in the ureteric bud and also in the tissue derived from the metanephric mesenchyme by the mesenchymal-epithelial transition (MET) [20]. We found that EpCAM$^+$TROP2$^-$ cells expressed Sall1, a marker of metanephric mesenchymal cells [26](Figure 2E), and that the number of EpCAM$^+$TROP2$^-$ cells increased from E12.5 to E14.5, corresponding to the timing of MET [27](Figure 2C). These results suggest that the EpCAM$^+$TROP2$^-$ population is mainly composed of epithelial cells derived from the metanephric mesenchyme.

Expression of TROP2 in ureteric buds

TROP2 is highly expressed in a variety of carcinomas and involved in cancer cell proliferation [11,28]. In kidney development, a previous study showed that cell proliferation is restricted mainly to the tip of the ureteric bud in fetal kidney, which corresponds to TROP2^{low} cells [17]. In fact, immunostaining of Ki67, a marker of cell proliferation, showed the expression to be higher in the tip cells than in the trunk cells (Figure S1). This result suggests that, unlike in carcinomas, the TROP2 expression level is not positively correlated with cell proliferation in fetal kidney.

Furthermore, in the corneal epithelia, TROP2 enhances the expression and localization of tight junctional proteins, including Claudin-1 and Claudin-7 [12]. However, immunostaining showed that in contrast to the gradient of TROP2 expression, Claudin-7 was uniformly expressed throughout the ureteric bud cells (Figure S2A). Moreover, Claudin-7 was found only in the lateral membrane of the ureteric duct, while TROP2 was located in both the lateral and basal membranes (Figure S2B). These results indicate that expression of TROP2 and Claudin-7 are not fully correlated in the fetal kidney, suggesting that TROP2 is not only involved in the formation of tight junctions in the ureteric bud.

The ureteric bud is surrounded by collagen-I in fetal kidney

The extracellular matrix (ECM) is important for the growth and branching morphogenesis of embryonic organs [29]. In fetal kidney, the ureteric bud and the collecting duct express low and high levels of collagen-binding integrins α1 and α2, respectively, suggesting collagen to play a role in the differentiation and maturation of the ureteric bud by binding to integrins [30,31]. Because trunk cells in the ureteric bud differentiate to form the collecting duct, we examined the expression of collagen and TROP2 in the developing kidney by immunostaining. In E14.5 kidney, type I collagen (collagen-I) was abundant surrounding the TROP2$^+$ trunks as well as in the mesenchyme and stroma around the ureteric bud trunk (Figure 3A). By contrast, little collagen-I was detected surrounding EpCAM$^+$ tip cells (Figure S3).

Integrins are major cell-surface receptors that mediate interactions between cells and the ECM and play a crucial role in various

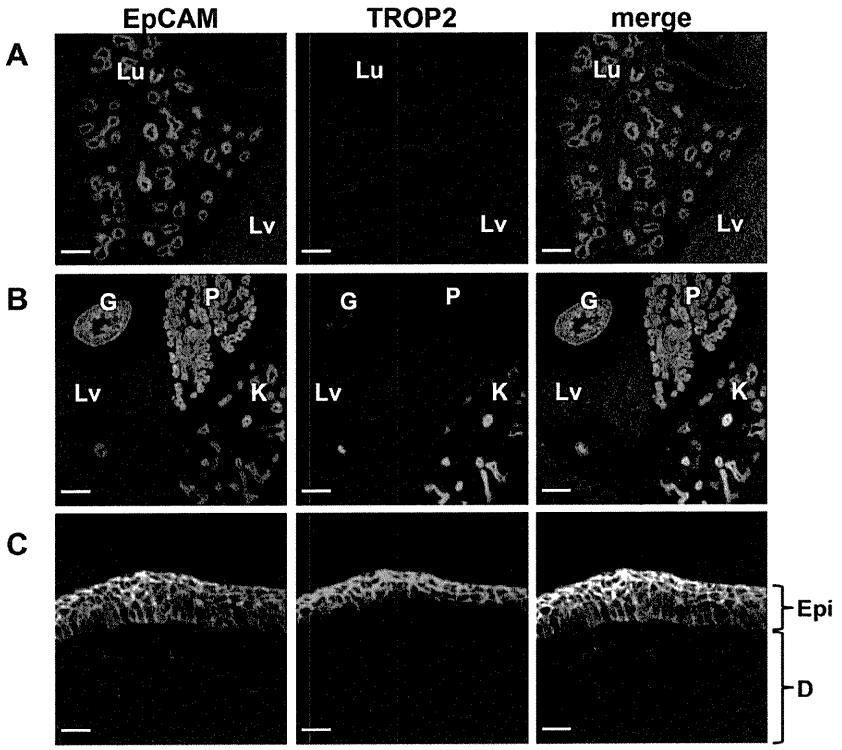

Figure 1. Expression of TROP2 and EpCAM in mouse at E14.5. (A–C) Immunostaining of E14.5 mouse frozen sections with anti-EpCAM (green) and anti-TROP2 (red) Abs. EpCAM was expressed in epithelial cells of various organs. By contrast, TROP2 expression was restricted to EpCAM^{+} cells in the kidney, gut and epidermis. L ; Lung, Lv ; Liver, P ; Pancreas, G ; Gut, K ; Kidney, Epi ; Epidermis, D ; Dermis, Scale bars = 200 μm.
doi:10.1371/journal.pone.0028607.g001

cellular functions such as adhesion, migration, proliferation and anti-apoptosis [32,33]. Integrins consist of α and β subunits, with the extracellular domain of the α subunit conferring their specificity. To compare the expression of collagen-binding integrins such as integrin α1β1 and integrin α2β1 between the trunk and tip cells in the ureteric bud, we performed a quantitative RT-PCR analysis of integrins using the sorted EpCAM^{+}TROP2^{low} and EpCAM^{+}TROP2^{high} cells from E14.5 kidney (Figure 3B). There was no significant difference in the levels of collagen-binding integrin subunits, α1, α2 and β1 between the trunk and tip cells, suggesting that the tip and trunk cells have a similar potential to bind collagen via integrins. Considering the co-localization of TROP2 and collagen-I at the basal membrane of the ureteric bud, TROP2 may play a role in the development of trunk cells such as branching by modulating the function of collagen-I.

Tip and trunk cells exhibit different potential to attach to and spread on collagen-I

To further characterize the collagen-binding properties of fetal ureteric bud cells, sorted tip and trunk cells in the ureteric buds were cultured on collagen-coated dishes. The numbers of cells attached to collagen-coated dishes were smaller for EpCAM^{+}TROP2^{high} cells than EpCAM^{+}TROP2^{low} cells, indicating that the trunk cells bind to collagen-I less efficiently (Figure 4A). Furthermore, while forward and side scatter by flow cytometry showed no significant difference in cell size between tip and trunk cells before plating (data not shown), the EpCAM^{+}TROP2^{low} cells were spread on the collagen-coated plates and exhibited membrane ruffles, resulting in an increase in cell size compared with the EpCAM^{+}TROP2^{high} trunk cells (Figure 4 B, C). It is known that new branches emerge from the tip and trunk cells form the mature ducts during the formation of ureteric bud branches, suggesting that the characteristics of tip and trunk cells in the same branch are different. These findings indicate that our primary cultures of ureteric bud cells recapitulate the differentiation process in vivo, i.e., the tip cells spread and migrate into the metanephric mesenchyme, whereas the differentiating trunk cells are less active.

Furthermore, although there was no difference in the expression of collagen-binding integrins between the tip and trunk cells in the ureteric bud, the potential of EpCAM^{+}TROP2^{high} trunk cells to attach to and spread on collagen-coated plates was low, suggesting that factors other than the integrins regulate the interaction between trunk cells and collagen-I. Because TROP2 was expressed at a higher level in the trunk than tip cells and co-localized with collagen-I in the basal membrane of ureteric ducts, TROP2 may affect the potential of trunk cells to adhere to collagen-coated plates.

TROP2 expression suppresses cell spreading

To reveal the role of TROP2 in the cell spreading on collagen-I, we sorted EpCAM^{+}TROP2^{low} cells and overexpressed TROP2 by expression vector in the primary culture. Compared with the control cells transfected with the empty vector, the size of cells overexpressing TROP2 was markedly reduced, strongly suggesting that TROP2 affects the potential of EpCAM^{+}TROP2^{low} tip cells to spread on collagen-I (Figure 4D, E).

To further confirm the role of TROP2 in the formation of ureteric bud branches, we utilized Madin-Darby canine kidney (MDCK) cells [34], established as a model for studying the

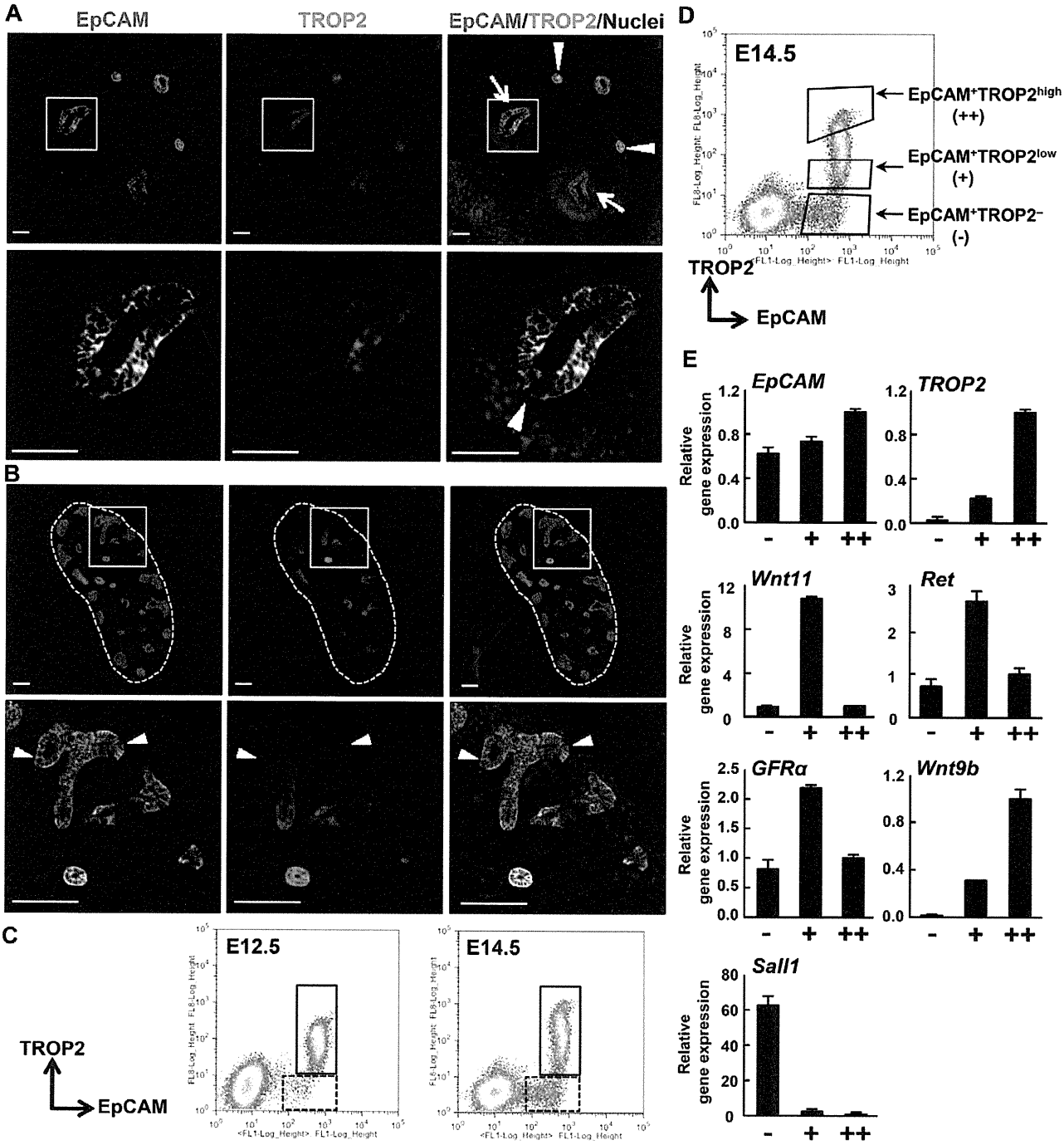

Figure 2. Characteristics of ureteric bud cells in the developing kidney. (A–B) Immunostaining of E11.5 (A) and E14.5 (B) kidney with anti-EpCAM (green) and anti-TROP2 (red) Abs and nuclei (blue). (A) Arrowheads indicate the Wolffian duct and the arrow indicates the ureteric bud. Higher magnification images of the boxed regions are shown underneath. In the lower figure of A, the ureteric bud grows toward the bottom and the yellow arrowhead indicates the tip of the ureteric bud. Scale bars = 50 μm. (B) The dotted line delineates the periphery of the kidney. Scale bars = 100 μm. (C) Flow cytometry of E12.5 and E14.5 kidney cells using anti-EpCAM and anti-TROP2 Abs. The boxed regions and the dotted boxed regions show TROP2^{+} and TROP2^{-} cell populations, respectively. (D) Fractionation of EpCAM+ cells in E14.5 kidney using anti-EpCAM and anti-TROP2 Abs. The upper, middle and lower boxed regions in the panel indicate the EpCAM^{+}TROP2^{high}, EpCAM^{+}TROP2^{low} and EpCAM^{+}TROP2^{nega} cell population, respectively. (E) Quantitative RT-PCR analysis of marker genes in freshly isolated E14.5 EpCAM^{+}TROP2^{nega}(−), EpCAM^{+}TROP2^{low}(+) and EpCAM^{+}TROP2^{high}(++) cells. The relative gene expression of marker/GAPDH is shown. Error bars are s.d.
doi:10.1371/journal.pone.0028607.g002